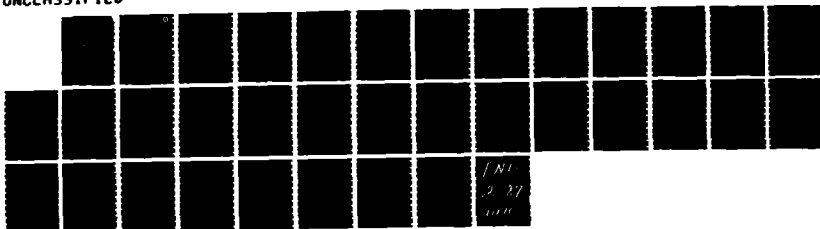THE INTERCHANGE INSTABILITY IN HIGH-LATITUDE PLASMA
BLOBS(U) NAVAL RESEARCH LAB WASHINGTON DC
P K CHATURVEDI ET AL   30 DEC 86 NRL-MR-5895

F/G 4/1

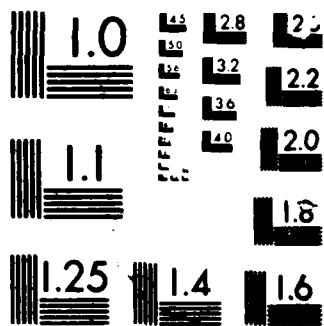NL

UNCLASSIFIED

AD-A176 242

The Interchange Instability in High-Latitude Plasma Blobs

P. K. CHATURVEDI AND J. D. HUBA

Geophysical and Plasma Dynamics Branch
Plasma Physics Division

JAN 3 0 1987

A

87   1

REPORT DOCUMENTATION PAGE

1a. REPORT SECURITY CLASSIFICATION			1b. RESTRICTIVE MARKINGS
UNCLASSIFIED			*AY76 242*

2a. SECURITY CLASSIFICATION AUTHORITY	3. DISTRIBUTION/AVAILABILITY OF REPORT
2b. DECLASSIFICATION/DOWNGRADING SCHEDULE	Approved for public release, distribution unlimited.

4. PERFORMING ORGANIZATION REPORT NUMBER(S)	5. MONITORING ORGANIZATION REPORT NUMBER(S)
NRL Memorandum Report 5895	

6a. NAME OF PERFORMING ORGANIZATION	6b. OFFICE SYMBOL (If applicable)	7a. NAME OF MONITORING ORGANIZATION
Naval Research Laboratory	Code 4780	

6c. ADDRESS (City, State, and ZIP Code)	7b. ADDRESS (City, State, and ZIP Code)
Washington, DC 20375-5000	

8a. NAME OF FUNDING/SPONSORING ORGANIZATION	8b. OFFICE SYMBOL (If applicable)	9. PROCUREMENT INSTRUMENT IDENTIFICATION NUMBER
ONR and DNA	(DAN) RAAE	

8c. ADDRESS (City, State, and ZIP Code)	10. SOURCE OF FUNDING NUMBERS			
	PROGRAM ELEMENT NO	PROJECT NO	TASK NO	WORK UNIT ACCESSION NO
Arlington VA 22217 Washington, DC 20305	62715H			DN580-072

11. TITLE (Include Security Classification)

The Interchange Instability in High-Latitude Plasma Blobs

12. PERSONAL AUTHOR(S)
Chaturvedi, P. K. and Huba, J. D.

13a. TYPE OF REPORT	13b. TIME COVERED		14. DATE OF REPORT (Year, Month, Day)	15. PAGE COUNT
Interim	FROM ___	TO ___	1986 December 30	35

16. SUPPLEMENTARY NOTATION   This research was partially sponsored by the Office of Naval Research and the Defense Nuclear Agency under Subtask W99QMXWA, work unit 00010 and work unit title "Plasma Structure Evolution."

17.	COSATI CODES		18. SUBJECT TERMS (Continue on reverse if necessary and identify by block number)
FIELD	GROUP	SUB-GROUP	Ionospheric structure, Radio scintillation mechanism
			Interchange instability High latitude ionosphere

19. ABSTRACT (Continue on reverse if necessary and identify by block number)

The stability of high latitude plasma density enhancements ("blobs") is analyzed with regard to the interchange mode (driven by a neutral wind or transverse electric field acting on the density gradient at the walls of the blobs). The effects arising from the finite parallel length of the blobs along the magnetic field lines are included in the analysis. Plasma regions of differing collisionalities, to which the blobs extend in altitude, are considered. We find that the finite-parallel blob size results in a modest reduction in the growth rates of the small (< 1 km) and intermediate (1-10 km) scale sizes, but severely reduces the growth rates for the large scale sizes (> 10 kms) for the observed parallel blob lengths (~ 300-600 kms). Further, it is found that the instability growth rates show a moderate reduction at higher altitudes (where ion-inertial effects may be dominant over the ion-neutral collisional effects). Thus, the $E \times B$ instability is considered a plausible candidate for the scintillation-causing irregularities (1-10 kms) associated with the high-latitude blobs.

20. DISTRIBUTION/AVAILABILITY OF ABSTRACT	21. ABSTRACT SECURITY CLASSIFICATION	
[X] UNCLASSIFIED/UNLIMITED ☐ SAME AS RPT. ☐ DTIC USERS	UNCLASSIFIED	
22a. NAME OF RESPONSIBLE INDIVIDUAL	22b. TELEPHONE (Include Area Code)	22c. OFFICE SYMBOL
J. D. Huba	(202) 767-3630	Code 4780

DD FORM 1473, 84 MAR   83 APR edition may be used until exhausted.   SECURITY CLASSIFICATION OF THIS PAGE
                                 All other editions are obsolete.

CONTENTS

DTIC
COPY
INSPECTED
1'

A-1

THE INTERCHANGE INSTABILITY IN HIGH-LATITUDE PLASMA BLOBS

I. INTRODUCTION

It has long been known that the ionosphere at high latitudes often displays density irregularities and structured electric fields which are of various magnitudes in scale and strength [Fejer and Kelley, 1980]. The recent resurgence in interest in high latitude irregularities has been due to the observation of scintillations by DNA's Wideband Satellite in association with the gradient in the total electron content (TEC) at these latitudes [Fremouw et al., 1977; Rino et al., 1978]. A variety of experimental techniques have now been employed to study the structure at high latitudes and its morphology is beginning to be understood better. On the basis of incoherent scatter radar returns, the plasma density contours have revealed the existence of high-latitude enhancements which have scale sizes transverse to and along the magnetic field on the order of hundreds of kms and have frequently been referred to as "blobs" [Vickrey et al., 1980; Kelley et al., 1982]. Simultaneous incoherent scatter and VHF scintillation measurements were used by Vickrey et al. (1980) to establish the co-location of ~ 1 km scale irregularities and the F layer blobs. Ground-based optical and digital ionosonde measure-ments, in conjunction with the particle measurements on the DE-2 satellite, have found the presence of large scale plasma irregularities (called "patches") at polar cap latitudes [Weber et al., 1984]. Various mechanisms have been proposed for the cause of these large-scale plasma irregularities, such as generation by particle precipitation and convection from other regions [Kelley et al., 1982; Kelley and Vickrey, 1984; Weber et al., 1984, Sojka and Schunk, 1986]. Associated with the large scale blobs, there are density gradients at "walls" of these blobs (primarily in the horizontal east-west direction) that are observed to be structured [Vickrey et al., 1980; Rino et al., 1983, Basu et al., 1984; Cerisier et al., 1985, Tsunoda et al., 1985]. It is generally believed that the structure at the so-called "intermediate" scale sizes (~ 1-10 kms) is responsible for the observed satellite scintillations.

A plasma blob at high latitudes is reminiscent of artificially released clouds in the ionosphere and this fact has motivated us to do analogous analysis of the $\underline{E} \times \underline{B}$ instability for the blob situation. In this connection, we mention that the $\underline{E} \times \underline{B}$ instability has been applied to the naturally occurring transverse density gradients at mid-latitudes [Scannapieco et al., 1975] and to the high-latitude situation [Keskinen and Ossakow, 1982; Keskinen and Ossakow, 1983; Mitchell et al., 1985]. In addition, we note here that yet another gradient-driven instability, the current convective instability (which occurs in presence of a parallel current) has been invoked to interpret high-latitude structure in situations which may be $\underline{E} \times \underline{B}$ stable [Ossakow and Chaturvedi, 1979; Chaturvedi and Ossakow, 1979; Huba and Ossakow, 1980; Chaturvedi and Ossakow, 1981]. Most of the past work for the $\underline{E} \times \underline{B}$ and current-convective instability was carried out in the approximation of an infinitely long blob parallel to the magnetic field. These earlier studies clearly need to be modified for the blob-related structure, since, as has been noted earlier, the blobs have finite length in the direction parallel to the field-lines. The work on the $\underline{E} \times \underline{B}$ instability in barium clouds has shown that the growth rate is severely modified for the long wavelength modes when the finite parallel size of the cloud is considered [Völk and Haerendel, 1971; Goldman et al., 1976; Sperling et al., 1984; Drake et al., 1985; Drake and Huba, 1986]. A similar analysis carried out for the current convective instability has demonstrated that the instability growth rate is reduced on the order of two orders of magnitude for the scintillation causing scale sizes (for the observed blob sizes) [Huba and Chaturvedi, 1986].

In this paper we investigate the $\underline{E} \times \underline{B}$ instability for the high latitude blob-like situation. Thus, in our analysis we have included the effects of the finite parallel blob size, and ion-inertia (which can become important at high altitudes where the ion-neutral collision frequency is small [Ossakow et al., 1978]). We find that the growth rate for the $\underline{E} \times \underline{B}$ instability is modified by the finite parallel size of the blob, with the longer wavelengths showing more severe reductions in growth rate than the small and intermediate scale sizes. The effect of ion-inertia at high altitudes also leads to a reduction in the growth rate, but the reduction is relatively moderate for the small and intermediate

wavelengths ($\lambda \leq 10$ km) but is substantial at the long wavelengths ($\lambda \geq 10$ km). Further, the mode is localized in the blob-region parallel to the magnetic field. This has some notable consequences. For instance, the mode may remain relatively unaffected by the regions afar. Thus, the blob-associated structure of F-region altitudes may develop even in the presence of a conducting E-region. The mapping of structure-associated potential fields is also modified due to the localization. The electrostatic potential is roughly constant within the enhancement (cloud) but as it maps into the background ionosphere, the mapping distance is finite due to the dissipation. This mapping, originally discussed by Farley [1959], follows the relationship $\left(L_{\parallel}/L_{\perp}\right) \propto \left(\sigma_{\parallel}/\sigma_{\perp}\right)^{1/2}$, where L is the characteristic field scalesize, σ is the conductivity of the medium, and the subscripts $\parallel$, $\perp$ refer to the parallel and transverse components to the magnetic field, respectively. We find that this mapping may not extend to large parallel distances for structured fields at higher altitudes where ν_{in} (and thus $\sigma_{\perp}$) is very small. We discuss these results in the final section.

The plan of the paper is as follows. In the next section, we present the basic equations and briefly discuss the equilibrium. In the third section, the nonlocal mode equation is derived. The fourth section contains the numerical results. Finally, in the fifth section the results are discussed.

II. BASIC EQUATIONS AND EQUILIBRIUM

A set of nonlinear equations describing the evolution of a plasma density enhancement has been derived in Sperling et al. [1984] and Drake et al. [1985]. We briefly present the derivation here. A plasma blob is assumed to have finite length along the uniform magnetic field $\underline{B} = B_0 \hat{z}$ with a background neutral wind $\underline{V}_n = V_n \hat{x}$. The plasma is assumed to be cold (i.e., $T = 0$); see Appendix A for a discussion of finite temperature effects. The basic equations are

$$\frac{\partial n}{\partial t} + \nabla \cdot \left(n\underline{v}_e\right) = 0 \tag{1}$$

$$0 = -e\underline{E} - \frac{e}{c}\,\underline{v}_e \times \underline{B} - m_e\nu_{en}\left(\underline{v}_e - \underline{V}_n\right) - m_e\nu_{ei}\left(\underline{v}_e - \underline{v}_i\right) \tag{2}$$

$$m_i\left(\frac{\partial}{\partial t} + \underline{v}_i \cdot \nabla\right)\underline{v}_i = e\underline{E} + \frac{e}{c}\,\underline{v}_i \times \underline{B} - m_i\nu_{in}\left(\underline{v}_i - \underline{V}_n\right) - m_i\nu_{ie}\left(\underline{v}_i - \underline{v}_e\right) \tag{3}$$

3

$$\nabla \cdot \underline{J} = \nabla \cdot [ne(\underline{v}_i - \underline{v}_e)] = 0 \tag{4}$$

$$\nabla \times \underline{B} = \frac{4\pi}{c} \underline{J} \tag{5}$$

In the above n_α and $\underline{v}_\alpha$ are the density and fluid velocity, respectively, of species α, $\nu_{\alpha n}$ is the α species - neutral collision frequency, ν_{ei} is the electron-ion collision frequency, ν_{ie} is the ion-electron collision frequency and α refers to electrons (e) or ions (i). The electric and magnetic fields are represented in terms of potentials as

$$\underline{E} = - \nabla\phi - \frac{1}{c} \frac{\partial A_z}{\partial t} \hat{z} \tag{6}$$

and

$$\underline{B} = B_0 \hat{z} + \nabla A_z \times \hat{z} \tag{7}$$

where ϕ is the electrostatic potential and A_z is the vector potential associated with the magnetic field produced by the self-consistent plasma currents. We consider only A_z since $J_\parallel \gg J_\perp$ and assume that $|\nabla A_z \times \hat{z}| \ll B_0$.

The electron motion transverse and parallel to B_0, is described as

$$\underline{v}_{e\perp} = - \frac{c}{B} \nabla_\perp \phi \times \hat{z} \tag{8}$$

and

$$v_{\parallel e} = - eE_\parallel / [m_e(\nu_e + f\nu_{ei})] \tag{9}$$

with

$$E_\parallel = - \nabla_\parallel \phi - \frac{1}{c} \frac{\partial A_z}{\partial t} \tag{10}$$

where $\nu_e = \nu_{ei} + \nu_{en}$ and $\nabla_\parallel = \hat{b} \cdot \nabla$, $\hat{b} = \underline{B}/|\underline{B}_0|$. Also, with $\nu_e/\Omega_e \ll 1$ and $\nu_{in} \lesssim \Omega_i$, $f = m_e\nu_{en}/m_i\nu_{in} \ll 1$. The ion dynamics is given by

$$\underline{v}_{i\perp} = \epsilon_i \left[- \frac{c}{B} \nabla_\perp \phi \times \hat{z} + \frac{\tilde{\nu}_{in}}{\Omega_i} \underline{v}_n \times \hat{z} - \frac{\tilde{\nu}_{in}}{\Omega_i} \frac{c}{B} \nabla_\perp \phi + \left(\frac{\tilde{\nu}_{in}}{\Omega_i}\right)^2 \underline{v}_n \right] \tag{11}$$

4

$$v_{\parallel i} = eE_{\parallel} \nu_{en} / [m_i \bar{\nu}_{in} (\nu_e + f\nu_{ei})] \tag{12}$$

where $\varepsilon_i = (1 + \nu_{in}^2/\Omega_i^2)^{-1}$ and $\bar{\nu}_{in} = \nu_{in} + \partial/\partial t$. In (11), both Pedersen and Hall responses to the electric field and neutral wind have been included. Note also that we have included the ion inertia ($\partial/\partial t$ in $\bar{\nu}_{in}$) in the above, even though the full convective derivative has not been included ($\underline{v} \cdot \nabla \underline{v}$ term is not taken into account). The reason for doing so is the fact that this term only introduces a real frequency to the solution and does not affect the stability criterion.

We present the equations derived by Sperling et al. [1984] for the $\underline{E} \times \underline{B}$ instability with the ion-inertial effects included. These equations, derived from (8)-(12) and (1), (4) and (5), are

$$\frac{dn}{dt} - \frac{c}{B} \nabla\hat{\phi} \times \hat{z} \cdot \nabla n + \nabla_{\parallel} \frac{c}{4\pi e} \nabla_{\perp}^2 A_z = 0 \tag{13}$$

$$\varepsilon_i \frac{c}{B} \frac{\bar{\nu}_{in}}{\Omega_i} \nabla_{\perp} \cdot n\nabla_{\perp}\hat{\phi} + \varepsilon_i \frac{c}{B} \frac{\bar{\nu}_{in}^2}{\Omega_i^2} \hat{z} \times \nabla\hat{\phi} \cdot \nabla n + \frac{\bar{\nu}_{in}}{\Omega_i} \hat{z} \times \underline{V}_{-n} \cdot \nabla n$$
$$+ \frac{c}{4\pi e} \nabla_{\parallel}\nabla_{\perp}^2 A_z = 0 \tag{14}$$

$$\nabla_{\perp}^2 A_z = \frac{4\pi}{cn_e} (\nabla_{\parallel}\hat{\phi} + \frac{1}{c} \frac{dA_z}{dt}) \tag{15}$$

where $\eta_e = m_e\nu_e/ne^2$ is the parallel resistivity and

$$\hat{\phi} = \phi - \frac{B}{c} \frac{\bar{\nu}_{in}}{\Omega_i} \underline{V}_{-n} \cdot \hat{x} \tag{16}$$

$$\frac{d}{dt} = \frac{\partial}{\partial t} + \frac{\bar{\nu}_{in}}{\Omega_i} \hat{z} \times \underline{V}_{-n} \cdot \nabla \tag{17}$$

$$\nabla_{\parallel} = \frac{\partial}{\partial z} + B_0^{-1}\nabla A_z \times \hat{z} \cdot \nabla \tag{18}$$

Equation (13) is the electron continuity equation, (14) is the charge conservation equation and (15) is the Ampere's law. Now we shall discuss the equilibrium of these equations briefly.

5

The equilibrium of a cold plasma enhancement has been discussed by Sperling et al. [1984]. A two-dimensional cloud localized along and across the magnetic field $\underline{B}_0$, $n_i = n_i(x,z)$ with $n_i \neq 0$ for $|x| \leq x_0$ and $|z| \leq z_0$ is described by equations

$$\frac{\partial n}{\partial t} + \frac{c}{4\pi e} \frac{\partial}{\partial z} \frac{\partial^2 A_z}{\partial x^2} = 0 \tag{19}$$

$$\epsilon_i \frac{c}{B} \frac{\nu_{in}}{\Omega_i} \frac{\partial}{\partial x} n \frac{\partial}{\partial x} \hat{\phi} + \frac{c}{4\pi e} \frac{\partial}{\partial z} \frac{\partial^2 A_z}{\partial x^2} = 0 \tag{20}$$

$$\frac{\partial^2 A_z}{\partial x^2} = \frac{4\pi}{cn_e} \left(\frac{\partial \hat{\phi}}{\partial z} + \frac{1}{c} \frac{\partial A_z}{\partial t} \right) \tag{21}$$

In the above, it has been assumed that the background ionosphere is uniform throughout the region, and x_0 and z_0 are, respectively, the typical transverse and longitudinal scales of the plasma enhancements. From (19)-(21) we find that the equilibrium is given by $A_z = \hat{\phi} = 0$ with $n(x,z)$ an arbitrary function. For simplicity we consider the plasma density to be given by

$$
\begin{aligned}
n(x,z) &= n_1 & z &< -z_0 \\
n(x,z) &= n_i(x) & -z_0 &< z < z_0 \\
n(x,z) &= n_2 & z &> z_0
\end{aligned}
\tag{22}
$$

III. LINEAR ANALYSIS AND DISPERSION RELATION

We perturb the set of equations (13)-(15) over the equilibrium discussed in the previous section and linearize the equations with respect to perturbations. The perturbed quantities are assumed to vary as $\tilde{f} \sim f(z) \exp(\gamma t + k_y y)$. The above set then leads to

$$(k_y^2 D_r + \gamma)\tilde{A}_z = -c \frac{\partial \tilde{\phi}}{\partial z} \tag{23}$$

$$\left[\gamma\left(1 + \frac{\gamma}{\nu_{in}}\right) - \gamma_0 \right] \tilde{\phi} = - \frac{\gamma \alpha D_r}{c} \frac{\partial \tilde{A}_z}{\partial z} \tag{24}$$

The above equations are the same as those discussed in the work of Sperling et al. [1984] with the exception of the second term in parenthesis on the left hand side of (24) $\left(\gamma/\nu_{in}\right)$ which represents the effects of ion inertia. The following definitions have been used in (23) and (24); $\gamma_0 = V_n/L_n$, $L_n = \left(\partial \ln n_i/\partial x\right)^{-1}$, $D_r = \nu_{ei} c^2/\omega_{pe}^2$, $\omega_{pe}^2 = 4\pi n_0 e^2/m_e$, $\alpha = \Omega_e \Omega_i/\nu_{ei}/\nu_{in}$, and $\nu_{in}/\Omega_i \ll 1$ was assumed. We discuss some well-known results from (23) and (24) in the local analysis in Appendix A. Now we present a derivation of the nonlocal dispersion relation.

The method of solving (23) and (24) we follow here is similar to that used in Sperling et al. [1984], Drake et al. [1985], and Huba and Chaturvedi [1986]. In the outer regions (outside the plasma blob), the ambient ionosphere is assumed to have no density gradient and a decaying solution is assumed for the modes in these regions. We shall distinguish between the two outside regions by their differing ambient parameters (density, ν_{in}, etc.). We refer to the region below the blob as the region 1 (bottomside) and the one above it as the region 2 (topside). In these regions, the solution is written as

$$\tilde{\phi} = \tilde{\phi}_1 e^{k_1 z}, \quad \tilde{A}_z = \tilde{A}_1 e^{k_1 z} \qquad z < -z_0,$$

$$\tilde{\phi} = \tilde{\phi}_2 e^{-k_2 z}, \quad \tilde{A}_z = \tilde{A}_2 e^{-k_2 z} \qquad z > z_0 \qquad (25)$$

The inverse of decay lengths of the mode-associated fields in the ambient ionosphere are given by

$$\frac{k_p^2}{k_y^2} = \left[\frac{\left(1 + \frac{\gamma}{\nu_{in}}\right)}{\alpha R}\right]_p \qquad p = 1,2 \qquad (26)$$

where

$$R = \frac{k_y^2 D_r}{\gamma + k_y^2 D_r} \qquad (27)$$

In the above p = 1,2 refer to the two outer regions as noted earlier, the term $\left(\gamma/\nu_{in}\right)$ in (26) describes the effects of ion inertia and R is a

measure of the electromagnetic effects. For the electrostatic case $(\kappa_y^2 D_r \gg \gamma)$, $R = 1$ and for the electromagnetic case $(\gamma \gg \kappa_y^2 D_r)$, $R = \kappa_y^2 D_r / \gamma \ll 1$.

Inside the blob, the mode is represented by a plane wave solution,

$$\bar{\phi} = \tilde{\phi}_i \, e^{ik_i z} \, , \quad \bar{A}_z = \tilde{A}_{zi} e^{ik_i z} \qquad -z_0 < z < z_0, \qquad (28)$$

with the parallel wavenumber of the mode inside the blob being given by

$$\frac{k_i^2}{k_y^2} = \left\{ \frac{[\gamma_0 - \gamma(1 + \frac{\gamma}{\nu_{in}})]}{\gamma} \frac{1}{\alpha R} \right\}_i \qquad (29)$$

where the quantities are evaluated in the blob region and the ion-inertial effects are represented by the third term in the numerator of (29). A solution is constructed from (29) for the mode, using the two roots of k_i ($k_{i\pm}$ corresponding to $\pm$ roots),

$$\bar{A}_i = \hat{A} \, e^{ik_{i+} z} + \hat{B} \, e^{ik_{i-} z} \qquad (30)$$

A similar solution is written out for $\bar{\phi}_i$. The solutions are matched at the boundaries of the inner and outer regions to derive the dispersion relation. The appropriate matching conditions are obtained by integrating (23) and (24) across the boundaries $(z = \pm z_0)$; it is found that $\bar{\phi}$ and $\bar{A}_z$ are continuous at $z = \pm z_0$. Using (25) and (30) in (23) and (24) with these matching conditions, we find the dispersion equation is

$$k_i z_0 = \frac{1}{2} \tan^{-1} \frac{\frac{k_1}{k_i} + \frac{k_2}{k_i}}{1 - \frac{k_1 k_2}{k_i^2}} + m\pi \qquad (31)$$

where m is an integer. The largest growth rate occurs for m = 0 mode and we consider only this mode henceforth. The wavenumbers $k_{1,2}$ and k_i are defined in (28) and (29), respectively. Equation (31) is solved numerically, but first we shall discuss some simple analytical results from it.

The results of local analysis can be obtained from (31) in the limit
... where $\hat{Y} = Y/Y_0$, in which case one may write tan $(2k_i z_0) =$
$2k_i z_0$ and the dispersion relation is

$$2k_i z_0 = \pi/2 \tag{32}$$

By identifying $k_{zeff}^2 = \pi^2/16z_0^2$, one is able to recover the local theory
results A7, A8 and A10-(A11) from (32).

The finite length of the blob and the ion inertia both contribute to
a reduction of the $\underline{E} \times \underline{B}$ instability growth rate. We have noted earlier
that we distinguish the ionospheric regions above and below the blob by
their differing ambient parameters. We shall also distinguish three
separate cases in which the effects of ion inertia are introduced
differently (see Tables 1 and 2). In case I, both the topside and the
bottomside ionosphere, as well as the blob correspond to ionospheric
altitudes where the ion-inertial effects are neglected. In the case II,
the ion inertial effects are introduced only in the topside ionosphere
region and in the case III, both the blob and the topside ionosphere are
considered at altitudes where ion-inertial effects may become important.
We present some simple analytical expressions for the growth rate of
the $\underline{E} \times \underline{B}$ instability for the above three cases in Appendix B. It is
shown there that the growth rate is reduced for a finite length blob and
the reduction is more pronounced at the long transverse wavelengths.
Also, the earlier results of Sperling et al. [1984] are recovered for the
case when the regions 1 and 2 may be approximated in the collisional limit
with the same parameters. We shall further discuss the results for the
three cases in the discussion section along with the numerical results
which will be presented next.

IV. NUMERICAL RESULTS

We have solved the nonlocal dispersion relation (31) for parameters
appropriate to the high latitude blob situation in three different cases
as described in the previous section. The parameters used have been
tabulated in Tables 1 and 2. We use the following normalizations:
$\hat{Y} = Y/Y_0$, $\hat{k}_y = k_y L_r$, $\hat{z}_0 = z_0/z_r$, $z_r^2 = \alpha_i L_{ri}^2$, and $L_r^2 = D_r/Y_0$. The blob
length, $2z_0$, has been assumed to be the same in the three cases and is

9

taken to be 300 kms. Similarly, the gradient scale length, L_N, associated with the "walls" of blob is taken to be 40 kms and the neutral wind velocity, V_n, is taken to be 400 m/sec in all the three cases, resulting in the linear local theory growth rate $\gamma_0 \sim 10^{-2}$ sec^{-1}. Most of the other parameters and symbols are explained in Tables 1 and 2 and will be stated when introduced below. In the following the growth rate expressions have been computed as a function of wavenumber, the blob length and the ion collision frequency for various cases. In addition, we have also plotted the wave function within and outside the blob for various cases, to display the localization of the mode around the instability region (i.e., the blob). For reference we note that 1 km modes correspond to $k_y L_r =$ 14.5 and 10 km modes correspond to $k_y L_r = 1.45$.

Figure 1 shows the normalized growth rate, γ/γ_0, plotted as a function of normalized transverse wavenumber, $k_y L_r$, for the three cases mentioned above. In case I (curve A), the bottomside, blob and topside are all taken to be collisional and ion inertial effects are unimportant. For large k_y (short transverse wavelengths), the growth rate can be seen to approach asymptotically the local theory growth rate, $\gamma = \gamma_0$. For small k_y (long transverse wavelengths), the growth rate is reduced. The inter- mediate scale size regime corresponding to the 1 - 10 km is of special interest, for these irregularities are associated with the signal scintillations. It can be seen that the finite blob length has little effect on the 1 km scalesize mode, where growth rate is close to the local theory value ($\gamma = 0.9 \gamma_0$) but at the 10 km scalesize-end, the growth rate is down by almost an order of magnitude ($\gamma = 0.2 \gamma_0$). When inertial effects are introduced for the topside (case II, curve B), the growth rate curve shows an overall decrease, and the reduction at long wavelengths becomes more pronounced. Thus the 1 km-end of intermediate scale size shows small reduction in growth rate ($\gamma = .75 \gamma_0$), while the 10 km wave- length modes suffer severe reduction ($\gamma = .05 \gamma_0$) in growth rate. This trend continues for the case when the inertial effects are important for both the blob and the topside (case III, curve C). Now even the local growth rate (in the inertial limit) is different from the value in the collisional case ($\gamma = 0.6 \gamma_0$ in the inertial case, while $\gamma = \gamma_0$ in the

collisional case). The 1 km-scales show less reduction in the growth rate
due to the finite blob length effects ($Y = 0.35 \, Y_0$) than the 10 km-size
scales ($Y = 0.025 \, Y_0$), as expected.

In Figs. 2a - 2b the explicit effect of finite blob size is shown on
the growth rates of 1 km- and 10 km-size modes for the cases I and III,
respectively. Figure 2a refers to case I, and we see that the 1 km scale
sizes (curve A) experience lesser reductions in the growth rate than the 10
km-size modes (curve B). It can be seen that for very long blobs
(approaching the infinitely long blob limit, or the local theory limit),
the growth rate for $k_y L_r = 14.5$ ($\lambda_\perp \sim 1$ km) approaches the local theory
value ($Y = Y_0$) and for small blob-lengths, the growth rate is progressively
reduced. This pattern is more pronounced for the longer wavelengths
($k_y L_r = 14.5$, $\lambda_\perp \sim 10$ kms) for which the growth rate in the infinite blob
limit ($Y = 0.8 \, Y_0$) is less than the local theory value, $Y = Y_0$ (which is
valid only for short wavelengths such that $k_y L_N \gg 1$). A similar trend is
found for growth rate behavior as a function of blob-length, when the
inertial effects are introduced. This is shown in Fig. 2b, and the
inertial effects have been included for both the blob and the topside
regions. The growth rates for both the scale sizes ($\lambda_\perp \sim 1$, 10 km) are
reduced in this (inertial) case for the infinite blob limit from the value
corresponding to the collisional limit. And as the blob lengths get
smaller, the reduction in the growth rate is more, with longer wavelengths
(curve B) showing more pronounced reduction than the small wavelengths
(curve A).

In Figs. 3 - 5 we have plotted the wave functions for the modes within
the blob (the instability region) and outside it (the ambient ionosphere)
to show the localization of the modes in the blob region and its extension
into the ambient ionosphere. In Fig. 3, the wave function is plotted for
the short wavelength mode ($k_y L_r = 14.5$, $\lambda_\perp \sim 1$ km). Figures 3a and 3b
refer, respectively, to cases I and II. It can be easily seen that in the
collisional bottomside region the mode extends to smaller distances in the
ambient ionosphere than the topside ionosphere where collisions are low.
This mapping, dependent on the ambient collisionality, shows for the
collisional topside (Fig. 3a) the mode extending to smaller distances than
the case in which the topside is assumed inertial (Fig. 3b).

11

The mapping of modes into the ambient ionosphere is also scale size dependent. This is shown in the Figs. 4 and 5. In Fig. 4, wavenumbers $k_y L_r = 14.5$ (Fig. 4a), and $k_y L_r = 1.45$ (Fig. 4b) are plotted for the case when all the regions are taken to be collisional (case I, Table 2). Clearly, the longer wavelengths extend farther into the background than the smaller wavelengths. In Fig. 5, which corresponds to the case in which the topside is assumed inertial (case III, Table 2), this pattern is repeated, with the potential fields mapping to larger distances on the topside (which is less collisional) than on the bottomside (which is more collisional). Again, as one would expect, this mapping is to larger distances for the longer wavelength modes (Fig. 5b, $k_y L_r = 1.45$) than for the small wavelength mode (Fig. 5a, $k_y L_r = 14.5$).

An interesting point to note from the Figs. 3 - 5 is that in the highly collisional bottomside region, the smaller scales do not map to large distances. Thus we see that the 1 km-size mode maps to less than the blob length, $z_0/2$ (~ 75 kms) in the collisional bottomside (Figs. 3a and 4a). This implies that this mode, depending on the altitude of the blob, may not be affected by a conducting E-region. A conducting E-region is, however, likely to affect the development of longer wavelengths ($\geq$ 10 kms), as is evident from Figs. 3b - 4b, where the modes extend to several times the blob length ($\geq$ 400 kms).

V. DISCUSSION

We have studied the effects of finite blob-length on the interchange instability applicable to high latitudes and have included the effects of finite ion inertia. The experimental observations indicate that the high-latitude blobs are of finite extent parallel to the magnetic field with typical scalesizes of a few hundreds of km [Tsunoda et al., 1985]. This means that they span regions of varying plasma parameters in altitude, e.g., the collision frequencies, density, etc. At high altitudes, the ion-neutral collision frequency, ν_{in}, decreases and therefore the ion-inertial effects need to be included for the interchange instability analysis [Ossakow et al., 1978]. The introduction of finite parallel blob-size in

the analysis means that one should consider the finite parallel wavelength effects $(k_\parallel \ne 0)$ on the development of the instability and it further implies that the coupling of the blob region to the ambient ionospheric regions should be taken into account.

There are some obvious similarities of dynamics between an artificial plasma cloud and a plasma blob in the ionosphere. Both represent a plasma density enhancement above the background, both are of finite dimensions and in both the cases their motion with respect to the background results in a steepened backside or a wall gradient which is observed to be striated or structured. Considering these common features, we have applied the theory of interchange instability developed for plasma clouds by Sperling et al. [1984] and Drake et al. [1985] to the blob situation, and have included the ion-inertial effects in the analysis. It may be pointed out that there are also some differences between the two situations. The clouds are relatively small in parallel size (tens of kms) as compared with the blob sizes (a few hundred kms) and have a sharper transverse density gradient. The constituent ions of clouds are also different (usually barium) from the background ions while in the case of the blobs, the two are the same. Due to the large sizes, blobs occupy regions of diverse *ionospheric properties* in altitude. Thus the plasma properties at the bottom and the top of a blob may be very different in terms of collisionality, temperature, density, etc. This also has an important implication on the profile of the blob (as opposed to that of a cloud in whose case this size is quite small, and thus the properties of the two ionospheric regions adjacent to the cloud are not as different). Even though we have considered a 'top hat' model of the blob in our analysis for simplicity, the real blob would be asymmetrical in altitude, with its boundary in the collisional bottomside remaining sharp over the time-scale of the structure development as opposed to the topside where this boundary would be relatively more diffuse with respect to the background.

The analytical and numerical work on the stability of blobs with respect to the interchange mode presented in the previous sections demonstrate that, as in the case of the plasma clouds, the finite parallel blob-length results in an overall reduction of the growth rate of the interchange instability from the infinite blob case value. This reduction

13

is proportional to the wavelength of the mode: the longer the wavelength, the larger the reduction in its growth rate. In addition, the effects of ion-inertia (important at high ionospheric altitudes) are found to reduce the interchange instability growth rate somewhat. The consideration of finite parallel blob-length implied that the effects of finite $k_\parallel$ be considered on the interchange instability. The parallel extent of the modes is proportional to the transverse wavelength in ionosphere and this relationship is roughly given by the relation, $(L_\parallel/L_\perp) \propto (\sigma_\parallel/\sigma_\perp)^{1/2}$, where L is the characteristic scale size, σ is the ionospheric conductivity, and, $\perp$ and $\parallel$ represent components perpendicular and parallel to the magnetic field respectively. Clearly, as one goes higher in altitude, $\sigma_\perp$ (which is proportional to ν_{in}) decreases and $\sigma_\parallel$ (which is proportional to ν_{ei}^{-1}) increases. Thus, with increasing altitude, a given transverse scale size mode extends to larger and larger parallel distances. This fact explains the more pronounced reduction of interchange instability at longer transverse wavelengths for the finite-length blob situation. As the mode extends out of the blob (the instability region) into the ambient ionosphere, it attempts to move plasma electrodynamically in these regions (where the density is uniform and this represents a drag for the system). As a result, the growth rate of the interchange process is reduced. For longer transverse wavelengths, the parallel extent of the mode is also larger, and thus the 'load' also higher for the circuit, and, therefore, the growth rate reduction is more. Another consequence of the relationship $(L_\parallel/L_\perp) \propto (\sigma_\parallel/\sigma_\perp)^{1/2}$ is the fact that the smaller and intermediate scale-sizes are localized to shorter parallel distances around the blob (the instability region). Hence, depending on the altitude where the blob is located, this localization may be small enough so that the mode does not extend to the E-region on the bottomside. This would mean that the E-region would have little impact on the development of the structuring process in the high-latitude F-region, whether or not the E-region is conducting. The satellite signal scintillations are generally believed to be caused by the intermediate scale sizes (few 100 m - few km) and for a set of typical parameters, we have found in our numerical results that this may indeed be the case [see Figs. 3a, 3b, 4a and 5a].

The long parallel extension of modes on the topside also means that the regions of low neutral density (and therefore low ν_{in}) are being traversed by these modes. Thus ion-inertial effects need to be included and this has an effect of reducing the interchange instability growth rate [Ossakow et al., 1978]. This reduction is also wavelength dependent, the larger transverse wavelengths experience higher reductions in the interchange growth rates (see Figs. 1 and 2, curves B and C, and also the nonlocal growth rate expressions (B5) and (B6)). However, the interchange process may proceed rather unimpeded at short and intermediate scales, with the reductions in the growth rates less than an order of magnitude even at higher (~ 450 kms) altitudes, a result in agreement with Ossakow et al. [1978] (see Figs. 1 and 2).

Thus we find that the interchange process associated with the high latitude finite-length blobs is severely hampered for long wavelengths ($\geq$ 10 km) due to finite blob-size, possible coupling to a conducting E-region on the bottomside, and due to inertial effects as modes couple to higher altitudes on the topside. On the other hand, the small and intermediate scale sizes ($\leq$ 1 km and 1 - 10 km, respectively) may still experience the process of interchange unhindered for the observed blob lengths (~ 300 km) for the F-region altitudes (i.e., at altitudes around 400 - 500 km). There is evidence that the high-latitude blobs may be displaying such structures (Rino et al., 1983; Cerisier et al., 1985; Tsunoda et al., 1985). Therefore we suggest that the observed structure in this range (1 - 10 km) may be due to the $\underline{E} \times \underline{B}$ interchange instability due to the ambient electric fields, or neutral winds, or a combination of both. We have not considered the possible origins of the large scale length structures (blobs, patches, etc.) observed at high latitudes in this work (scales sizes $\geq$ 100 kms); on the basis of this work, these are produced by some other mechanism than the interchange process. We have also not attempted to include the dynamics of these large structures or their realistic profiles. The interchange process discussed here develops over a time scale of minutes (~ 10^2 sec) whereas the long scale size variations occur over a period of hours, thus making the assumption of a 'static' blob valid to lowest order.

In conclusion, we have argued that for the finite-length blobs in the high latitude F-region, the intermediate scale size structure responsible for satellite scintillations may be caused by the $\underline{E} \times \underline{B}$ interchange instability, even in the presence of a conducting E-region (for the blob sizes of ~ 300 km). We have also shown that for these scale sizes (1 - 10 km) the effect of ion-inertia introduces modest reductions in the interchange instability growth rates. All these effects (finite blob length, effect of inertia, etc.) however act to reduce the growth rate of the interchange instability at long scales (>> 10 km) severely, thus making it unlikely that the large scale sizes would be locally produced by the interchange process in high-latitude F-region.

ACKNOWLEDGMENTS

REFERENCES

Basu, B. and B. Coppi, Localized plasma depletion in the ionosphere and the equatorial Spread F, Geophys. Res. Lett., 10, 900, 1983.

Basu, S., S. Basu, E. MacKenzie, W.R. Coley, W.B. Hanson, and C.S. Lin, F region electron density irregularity spectra near auroral acceleration and shear regions, J. Geophys. Res., 89, 5554, 1984.

Cerisier, J.C., J.J. Berthelier, and C. Beghin, Unstable density gradients in the high-latitude ionosphere, Radio Science, 20, 755, 1985.

Chaturvedi, P.K. and S.L. Ossakow, Nonlinear stabilization of the $\underline{E} \times \underline{B}$ gradient drift instability in ionospheric plasma clouds, J. Geophys. Res., 84, 419, 1979.

Chaturvedi, P.K. and S.L. Ossakow, Nonlinear stabilization of the current convective instability in the diffuse aurora, Geophys. Res. Lett., 6, 957, 1979.

Chaturvedi, P.K. and S.L. Ossakow, The current convective instability as applied to the auroral ionosphere, J. Geophys. Res., 86, 4811, 1981.

Chu, C., M.S. Chu, and T. Ohkawa, Magnetostatic mode and cross-field transport, Phys. Rev. Lett., 41, 653, 1978.

Drake, J.F., J.D. Huba, and S.T. Zalesak, Finite temperature stabilization of the gradient drift instability in barium clouds, J. Geophys. Res., 90, 5227, 1985.

Drake, J.F. and J.D. Huba, Convective stabilization of ionospheric plasma clouds, J. Geophys. Res., 91, 10108, 1986.

Farley, D.T., Jr., A theory of electrostatic fields in a horizontally stratified ionosphere subject to a vertical magnetic field, J. Geophys. Res., 64, 1225, 1959.

Fejer, B.G. and M.C. Kelley, Ionospheric irregularities, Rev. Geophys. Space Phys., 18, 401, 1980.

Fremouw, E.J., C.L. Rino, R.C. Livingston, and M.C. Cousins, A persistent subauroral scintillation enhancement observed in Alaska, Geophys. Res. Lett., 4, 539, 1977.

Goldman, S.R., L. Baker, S.L. Ossakow, and A.J. Scannapieco, Striation formation associated with barium clouds in an inhomogeneous ionosphere, J. Geophys. Res., 81, 5097, 1976.

Huba, J.D. and S.L. Ossakow, Influence of magnetic shear on the current convective instability in the diffuse aurora, J. Geophys. Res., 85, 6874, 1980.

Huba, J.D. and P.K. Chaturvedi, The effect of finite "blob" size on the current convective instability in the auroral ionosphere, J. Geophys. Res., 91, 7125, 1986.

Kelley, M.C., J.F. Vickrey, C.W. Carlson, and R. Torbert, On the origin and spatial extent of high-latitude F region irregularities, J. Geophys. Res., 87, 4469, 1982.

Kelley, M.C. and J.F. Vickrey, F-region ionospheric structure associated with antisunward flow near the dayside polar cusp, Geophys. Res. Lett., 1, 9, 907-910, 1984.

Keskinen, M.J. and S.L. Ossakow, Nonlinear evolution of plasma enhancements in the auroral ionosphere: Long wavelength irregularities, J. Geophys. Res., 87, 144, 1982.

Keskinen, M.J. and S.L. Ossakow, Nonlinear evolution of convecting plasma enhancements in the auroral ionosphere 2: Small scale irregularities, J. Geophys. Res., 88, 474, 1983.

Mitchell, H.G., Jr., J.A. Fedder, M.J. Keskinen, and S.T. Zalesak, A simulation of high latitude F-layer instabilities in the presence of magnetosphere-ionosphere coupling, Geophys. Res. Lett., 12, 283, 1985.

Ossakow, S.L., P.K. Chaturvedi, and J.B. Workman, High-altitude limit of the gradient drift instability, J. Geophys. Res., 83, 2691, 1978.

Ossakow, S.L. and P.K. Chaturvedi, Current convective instability in the diffuse aurora, Geophys. Res. Lett., 6, 332, 1979.

Rino, C.L., R.C. Livingston, and S.J. Mathews, Evidence for sheet-like auroral ionospheric irregularities, Geophys. Res. Lett., 5, 1039, 1978.

Rino, C.L., R.C. Livingston, R.T. Tsunoda, R.M. Robinson, J.F. Vickrey, C. Senior, M.D. Cousins, J. Owen, and J.A. Klobuchar, Recent studies of the structure and morphology of auroral zone F region irregularities, Radio Science, 18, 1167, 1983.

Scannapieco, A.J., S.R. Goldman, S.L. Ossakow, D.L. Book, and B.E. McDonald, Theoretical and numerical simulation studies of mid-latitude F region irregularities, NRL Memo Rept. 3014, 1975.

Sojka, J.J. and R.W. Schunk, A theoretical study of the production and decay of localized electron density enhancements in the polar ionosphere, J. Geophys. Res., 91, 3245, 1986.

Sperling, J.L., J.F. Drake, S.T. Zalesak, and J.D. Huba, The role of finite parallel length on the stability of barium clouds, J. Geophys. Res., 89, 10913, 1984.

Tsunoda, R.T., I. Häggström, A. Pellinen-Wannberg, Å. Steen, and G. Wannberg, Direct evidence of plasma density structuring in the auroral F region ionosphere, Radio Science, 20, 762, 1985.

Vickrey, J.F., C.L. Rino, and T.A. Potemra, Chatanika/TRIAD observations of unstable ionization enhancements in the auroral F-region, Geophys. Res. Lett., 7, 10, 789-792, 1980.

Völk, H.J. and G. Haerendel, Striations in ionospheric ion clouds, 1, J. Gephys. Res., 76, 4541, 1971.

Weber, E.J., J. Buchau, J.G. Moore, J.R. Sharber, R.C. Livingston, J.D. Winningham, and B.W. Reinisch, F layer ionization patches in the polar cap, J. Geophys. Res., 89, 1683, 1984.

APPENDIX A: LOCAL THEORY

We Fourier analyze the perturbed quantities in the z-direction $\bar{f}(z) \sim \bar{f} \exp\left(ik_z z\right)$ for the local approximation. Then (23)-(24) result in the dispersion relation

$$\left[\gamma + k_y^2 D_r\right]\left[\gamma\left(1 + \frac{\gamma}{\nu_{in}}\right) - \gamma_0\right] = -\left(\gamma \alpha D_r\right)k_z^2 \tag{A1}$$

The effects of finite parallel wavelength are included on the right-hand side in the above. We first discuss the case $k_z = 0$, and later would consider the case when $k_z \neq 0$.

(a) $k_z = 0$

Setting $k_z = 0$ in (A1) leads to the dispersion relation

$$\left[\gamma + k_y^2 D_r\right]\left[\gamma\left(1 + \frac{\gamma}{\nu_{in}}\right) - \gamma_0\right] = 0 \tag{A2}$$

This equation has solution for a damped hydromagnetic mode, $\gamma = -k_y^2 D_r$, [Chu et al., 1978] and the other solution refers to the $\underline{E} \times \underline{B}$ instability including the ion-inertial effects [Ossakow et al., 1978]

$$\gamma\left(1 + \frac{\gamma}{\nu_{in}}\right) - \gamma_0 = 0 \tag{A3}$$

The two limits discussed in Ossakow et al. [19??] are the collisional and inertial limits for the solution of the quadratic in (A3). In the collisional limit, $\nu_{in} \gg 4\gamma_0$, one obtains the well-known result of local theory growth rate of the $\underline{E} \times \underline{B}$ instability for barium clouds,

$$\gamma = \gamma_0 \tag{A4}$$

In the inertial limit, the growth rate of the $\underline{E} \times \underline{B}$ instability is reduced from the collisional case, though not directly proportional to a decrease in ν_{in} (as might be expected at first), but proportional to $\sqrt{\nu_{in}}$ instead [Ossakow et al., 1978]. Thus, for $\nu_{in} < 4\gamma_0$, the growth rate is

$$\gamma = \sqrt{\gamma_0 \nu_{in}} \tag{A5}$$

20

(b) $k_z \neq 0$

We discuss the collisional and inertial limits in finite k_z approximation for the electrostatic and electromagnetic regimes.

(i) Electrostatic regime $(k_y^2 D_r \gg \gamma)$

In an electrostatic approximation the dispersion relation (A1) reduces to

$$\gamma^2 + \gamma \nu_{in}\left(1 + \alpha \frac{k_z^2}{k_y^2}\right) - \gamma_0 \nu_{in} = 0 \qquad (A6)$$

The collisional limit corresponds to $4\gamma_0 \ll \nu_{in}(1 + \alpha k_z^2/k_y^2)$, and the growth rate is

$$\gamma = \gamma_0 / \left(1 + \alpha \frac{k_z^2}{k_y^2}\right) \qquad (A7)$$

Clearly, the parallel dissipative electron motion has an overall effect of reducing the growth rate in this limit.

The inertial limit is $4\gamma_0 \gg \nu_{in}(1 + \alpha k_z^2/k_y^2)$ and the growth rate in this case is

$$\gamma = \sqrt{\gamma_0 \nu_{in}} - \frac{\nu_{in}}{2}\left(1 + \alpha \frac{k_z^2}{k_y^2}\right) \qquad (A8)$$

(ii) Electromagnetic regime $(\gamma \gg k_y^2 D_r)$

In this case, due to inductive effects, the mode couples to a parallel propagating Alfvén wave which has a stabilizing influence on the instability. The dispersion relation is now

$$\gamma^2 + \nu_{in}\gamma - \left(\gamma_0 \nu_{in} - V_A^2 k_z^2\right) = 0 \qquad (A9)$$

The growth rate in the collisional limit is

$$\gamma = \gamma_0 - V_A^2 k_z^2 / \nu_{in} \qquad (A10)$$

21

This expression is also given in Sperling et al. [1984] and by Basu and Coppi [1983]. In the inertial regime, the growth rate is

$$\gamma = \sqrt{\gamma_0 \nu_{in} - V_A^2 \kappa_z^2} \tag{A11}$$

where $V_A = (B_0^2/4\pi m_i n_0)^{1/2}$ is the Alfvén speed in the above.

iii) Finite temperature effects

Inclusion of finite temperature effects (i.e., $T \neq 0$) results in an additional stabilizing term. The growth rate in the electrostatic limit is given by

$$\gamma = (\gamma_0 - \kappa_z^2 T/m_e \nu_{ei})/(1 + \alpha k_z^2/\kappa_y^2) \tag{A12}$$

(see (36) of Drake et al., 1985). If we take $k_z \sim \pi/4z_0$ (see Section III), $z_0 = 150$ km, $T = T_e + T_i = 0.2$ eV, and $\nu_{ei} = 10^4$ sec^{-1}, we find that $\kappa_z^2 T/m_e \nu_{ei} \sim 2 \times 10^{-4}$ sec$^{-1} \ll \gamma_0 \sim 10^{-2}$ sec. Thus, finite temperature effects are unimportant for the parameters we consider. However, for sufficiently short wavelength modes it can be shown that finite temperature effects stabilize the mode (Drake et al., 1985).

APPENDIX B: NONLOCAL THEORY

We can rewrite the nonlocal dispersion relation (31) in terms of the normalized parameters as

$$\tan 2k_\perp z_0 = \left(\frac{1 - \hat{\gamma}\dfrac{\nu_{in}}{\nu_{in}}}{\hat{\gamma}_1}\right)_1^{1/2} \frac{\left[\left(\dfrac{\hat{\nu}_{in}}{\nu_{in}^\alpha}\right)_1^{1/2} + \left(\dfrac{\hat{\nu}_{in}}{\nu_{in}^\alpha}\right)_2^{1/2}\right]}{\left(\dfrac{1 - \hat{\gamma}\nu_{in}/\nu_{in}}{\hat{\gamma}_\alpha}\right)_1 - \left(\dfrac{\hat{\nu}_{in}}{\alpha\nu_{in}}\right)_1^{1/2}\left(\dfrac{\hat{\nu}_{in}}{\alpha\nu_{in}}\right)_2^{1/2}} \tag{31}$$

where $\hat{\nu}_{in} = \nu_{in} - \gamma$.

For finite size blobs and at higher altitudes, the reduced growth rate implies $\hat{\gamma} \ll 1$ and in this limit, one may take $\tan 2k_\perp z_0 = 2k_\perp z_0$. Then the dispersion relation becomes

$$2\hat{z}_0(\hat{\gamma} + \hat{k}_y^2)^{1/2} = \frac{\hat{\gamma}\left[\sqrt{a_1} + \left(1 + \dfrac{\hat{\gamma}}{\nu_{in2}}\right)^{1/2}\sqrt{a_2}\right]}{\left[1 - \hat{\gamma}\left\{\left(1 + \dfrac{\hat{\gamma}}{\bar{\nu}_{in1}}\right) + \sqrt{a_1 a_2}\left(1 + \dfrac{\hat{\gamma}}{\bar{\nu}_{in2}}\right)^{1/2}\right\}\right]} \tag{32}$$

where $a_n = x_1/x_n$, $x_n = \Omega_e\Omega_i/\nu_{ei}^{(n)}\nu_{in}^{(n)}$, $\bar{\nu}_{in} = \nu_{in}/\gamma_0$. In the above we have ignored the ion-inertial effects for the bottomside region (1) but retained them for the blob and the topside region (2). Now we write down analytical expressions for the growth rate when $\hat{z}_0$ is small.

Case I:

When both the topside and bottomside regions and the blob are collisional, the growth rate is

$$\hat{\gamma} = \frac{2\hat{z}_0\hat{k}_y}{(\sqrt{a_1} + \sqrt{a_2})} \tag{33}$$

where a_1 and a_2 represent the fact that we have considered different collisionalities for all the three regions. If one considers the

situation in which both the topside and bottomside regions may be approximated to be the same, then one obtains the result presented by Sperling et al. [1984]

$$\hat{\gamma} = (\hat{z}_0 \hat{k}_y)/\sqrt{a} \tag{B4}$$

Case II:

In this case, the bottomside and the blob are assumed collisional but the topside is considered inertial $(\nu_{in2} < \gamma_0)$, then the growth rate is given as

$$\hat{\gamma} = \frac{2\hat{z}_0 \hat{k}_y}{(\sqrt{a_1} + \sqrt{a_2/\bar{\nu}_{in2}})} \tag{B5}$$

where $\bar{\nu}_{in2} = \nu_{in2}/\gamma_0 < 1$.

Case III:

In this case, the bottomside is considered collisional but the ion-inertial effects are included for both the topside region and the blob. Then the growth rate is

$$\hat{\gamma} = (\hat{z}_0 \hat{k}_y)/\{(\sqrt{a_1} + \sqrt{\frac{a_2 \hat{\gamma}_1}{\bar{\nu}_{in2}}} /2\} \tag{B6}$$

where

$$\hat{\gamma}_1 = \sqrt{\bar{\nu}_{in1}}, \ (\gamma_1 = \sqrt{\gamma_0 \nu_{in_1}}) \tag{B7}$$

24

TABLE 1

IONOSPHERIC PARAMETERS[†]

	BOTTOMSIDE*	CASE I BLOB	CASE I TOPSIDE	CASE II BLOB	CASE II TOPSIDE	CASE III BLOB	CASE III TOPSIDE
Plasma Density cm^{-3} (n)	5×10^5	5×10^6	10^6	5×10^6	5×10^5	5×10^6	10^5
Electron-Ion Collision Frequency (ν_{ei})	10^3	10^4	5×10^3	10^4	10^3	10^4	5×10^2
Plasma Frequency (ω_{pe})	3.78×10^7	1.26×10^8	5.64×10^7	1.26×10^8	3.78×10^7	1.26×10^8	1.78×10^7
Ion-Neutral Collision Frequency (ν_{in})	30	0.5	0.05	0.1	0.01	0.05	0.01
$\alpha = (\Omega_e \Omega_i / \nu_{ei} \nu_{in})$	10^5	6×10^5	1.2×10^7	3×10^6	3.10^8	6×10^6	6×10^8
$D_r = \nu_e c^2/\omega_{pe}^2$		5.625×10^8					
$L_r = (D_r/\gamma_0)^{1/2}$		2.37×10^5					
$z_r = \sqrt{\alpha} \, L_r$	1.84×10^8		4.1×10^8		5.8×10^8		
$\hat{z}_0 = z_0/z_r$	.16		.07		.05		

[†] Some common parameters that have been used are: $T_e = T_i = 0.1$ eV; $B_0 = 0.5$ Gauss; $\Omega_e = 10^7$, $\Omega_i = 3 \times 10^2$, $L_N = 4 \times 10^6$ cm, $\gamma_0 = V_n/L_n = 10^{-2}$ sec^{-1}; $2z_0 = 300$ km.

* Bottomside parameters have been chosen to be the same for all three cases.

TABLE 2

PARAMETERS USED IN NUMERICAL COMPUTATION

	CASE I	CASE II	CASE III
a_1/a_1	6	30	60
a_1/a_2	.05	.01	.01
$\bar{\nu}_{11} = \nu_{in}^{(1)}/\gamma_0$	3000	3000	3000
$\bar{\nu}_1^{(1)} = \nu_{in}^{(1)}/\gamma_0$	50	10	5
$\bar{\nu}_{12} = \nu_{in}^{(2)}/\gamma_0$	5	1	0.1*
$\hat{z}_0$	0.2	.1	.05

* Notice that a_2 was computed using the value $\bar{\nu}_{in2} = 1$.
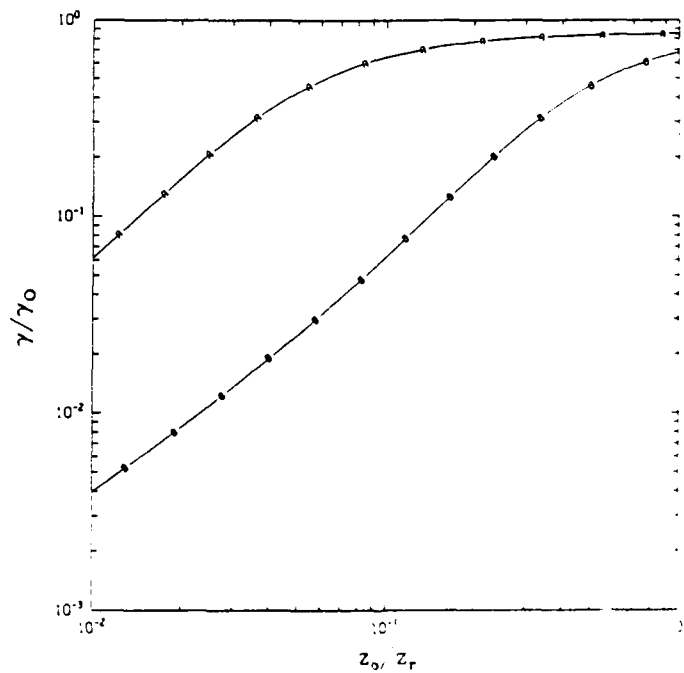
26
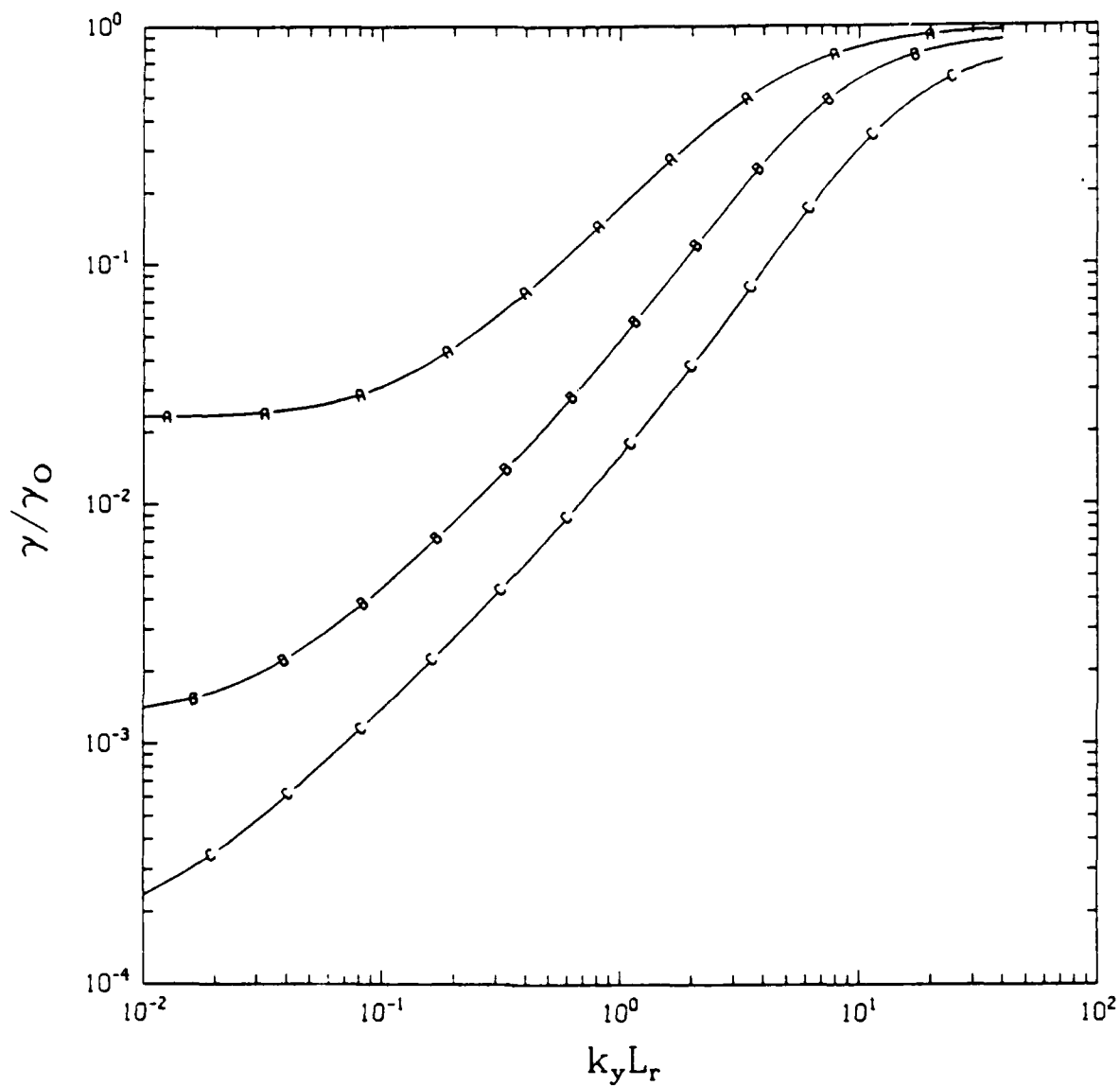
Fig. 1) Plot of the normalized growth rate γ/γ_0 vs. normalized transverse wavenumber $k_y L_r$ for the parameters listed in Table 2. Curve A corresponds to case I, curve B to case II, and curve C to case III.
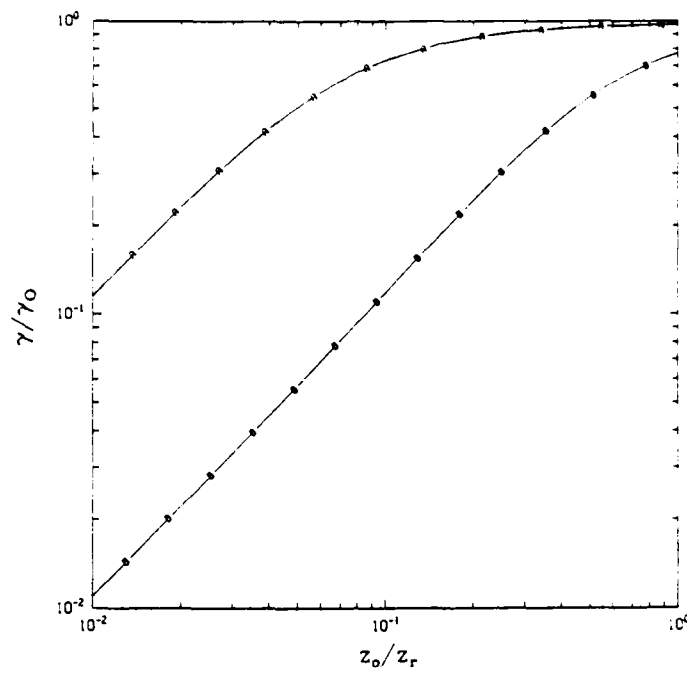
(a)

(b)

Fig. 2) Plot of the normalized growth rate γ/γ_0 vs. normalized parallel blob length z_0/z_r. Curve A corresponds to $k_y L_r = 14.5$ and curve B corresponds to $k_y L_r = 1.45$. (a) Parameters used are for case I. (b) Parameters used are for case III.
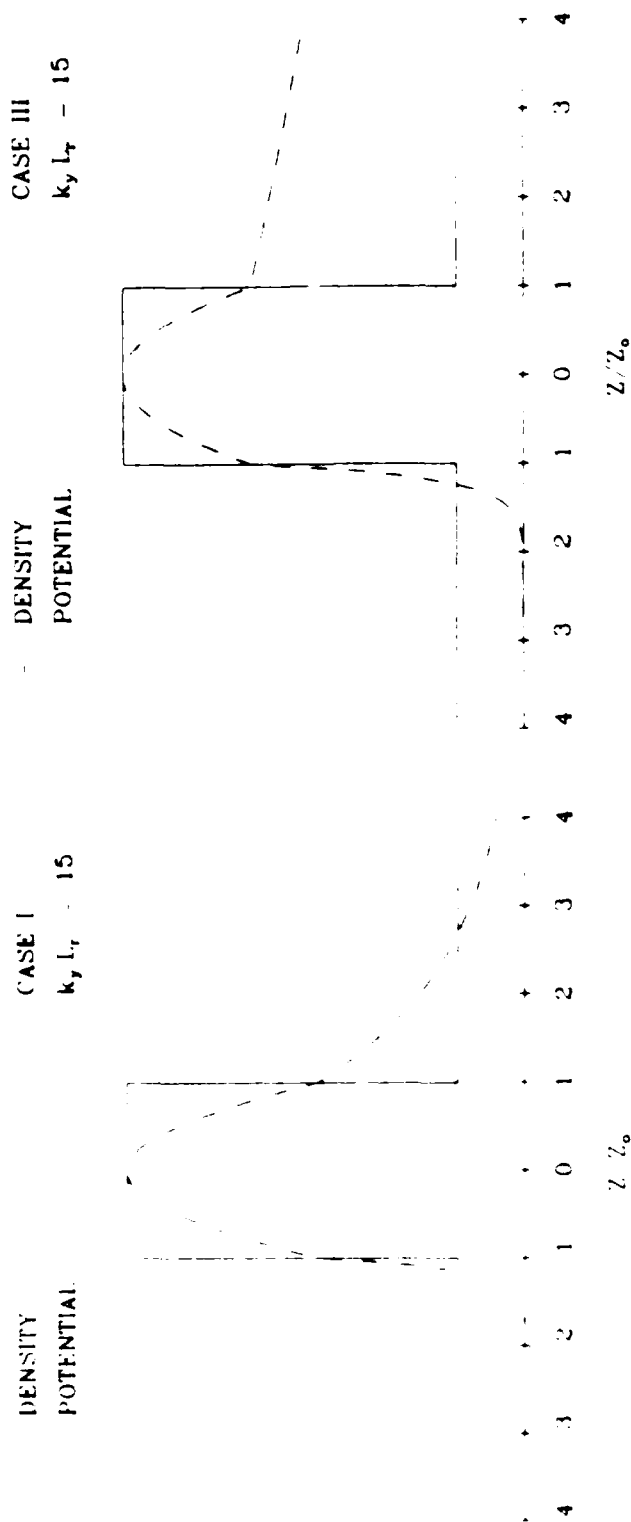
DENSITY
POTENTIAL

CASE III
$k_y L_r = 15$

Z/Z_o

(b)

CASE I
$k_y L_r = 15$

Z/Z_o

(a)

DENSITY
POTENTIAL

Fig. 9 Plot of density (solid line) and potential (dashed line) profiles as a function of blob length (z_0/z_r). (a) Parameters used are for Case I with $k_y L_r = 14.5$. (b) Parameters used are for Case III with $k_y L_r = 14.5$.

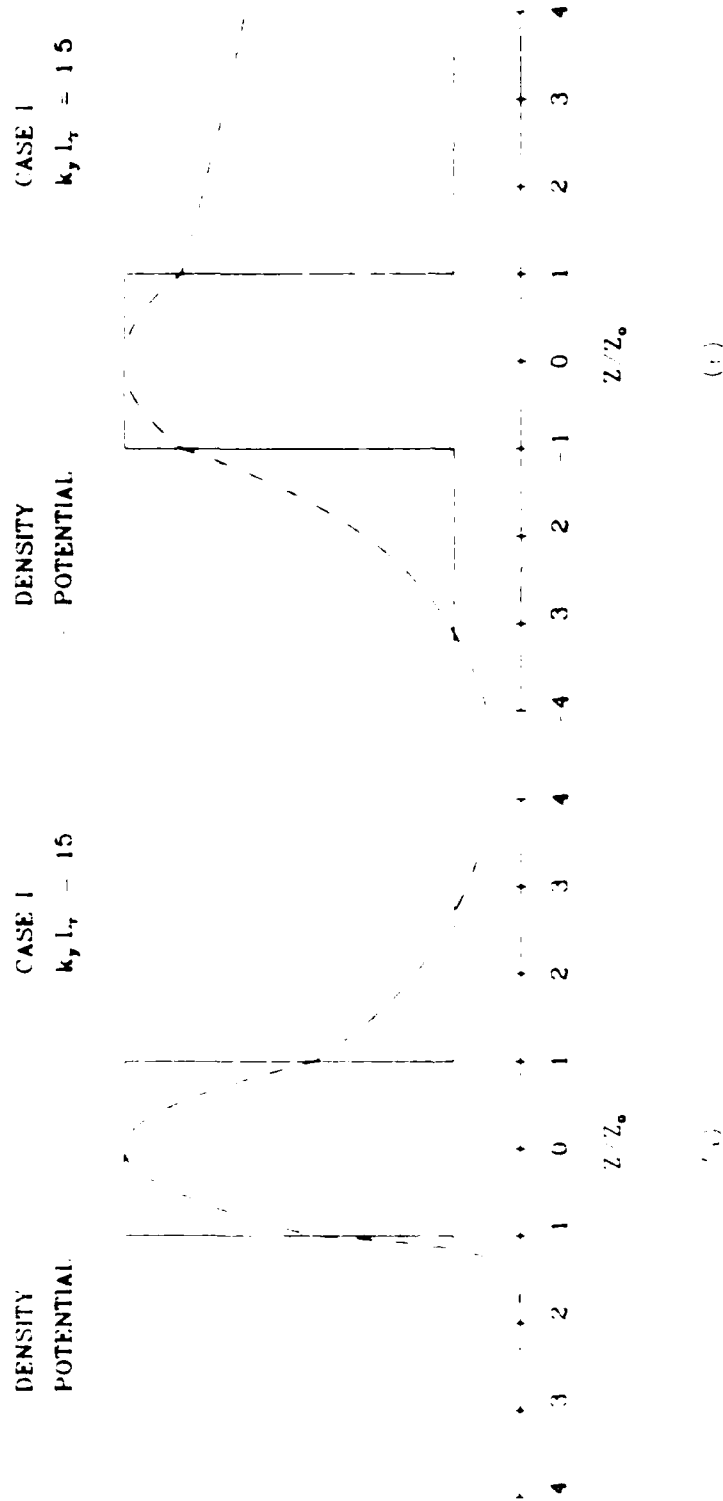CASE 1
$k_y L_r = 15$

DENSITY
POTENTIAL

Z/Z_0

(b)

CASE 1
$k_y L_r = 15$

DENSITY
POTENTIAL

Z/Z_0

(a)

Fig. plot of density (solid line) and potential (dashed line) profiles as a function of field length (z_0/z_p). The parameters used are for case 1. (a) $k_y L_r = 14.5$; (b) $k_y L_r = 1.45$.
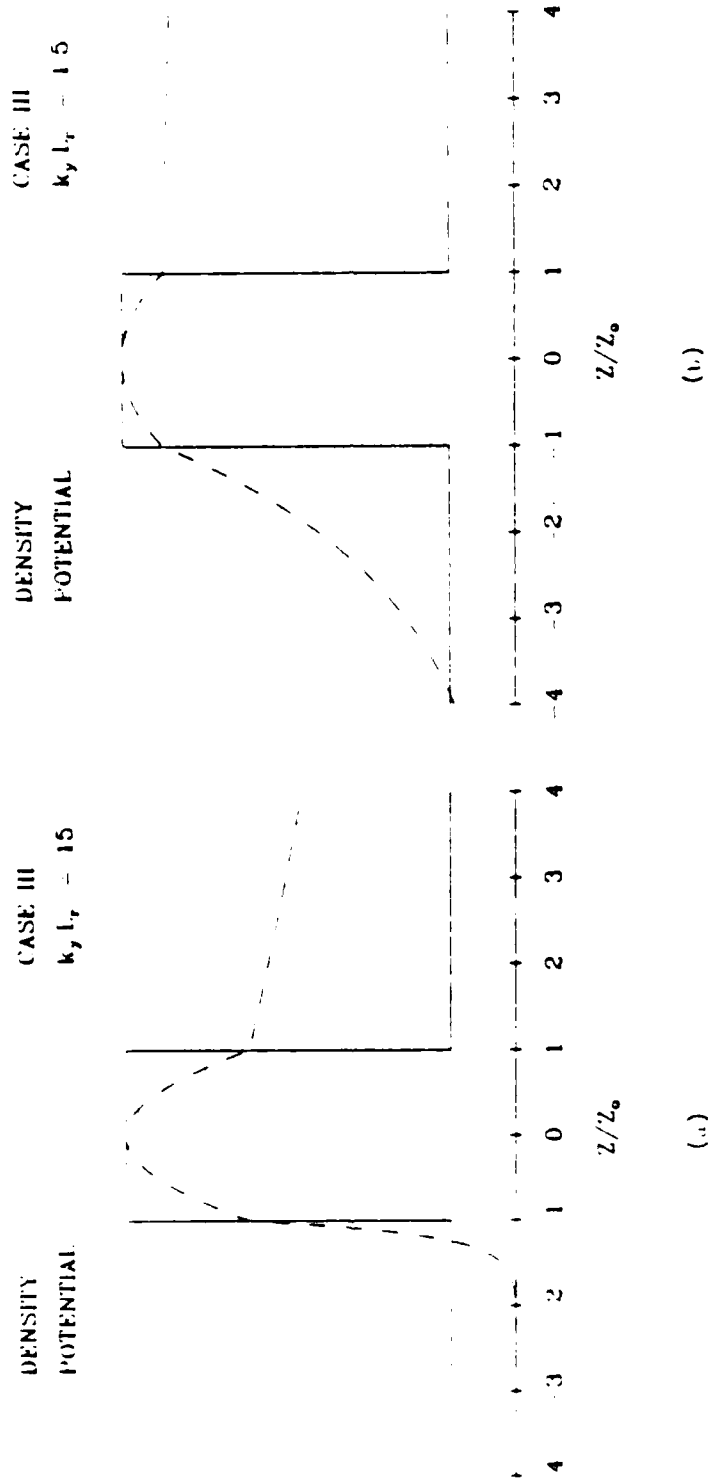
50

Fig. 5) Plot of density (solid line) and potential (dashed line) profiles as a function of blob length (z_0/z_t). The parameters used are for Case III. (a) $k_y l_r = 14.5$; (b) $k_y l_r = 1.45$.

END

2-87

DTIC